Tetrahedron 70 (2014) 1274–1282

Contents lists available at ScienceDirect

Tetrahedron

journal homepage: www.elsevier.com/locate/tet

Novel organogelators based on pyrazine-2,5-dicarboxylic acid derivatives and their mesomorphic behaviors

Yao-Dong Huang *, Wei Tu, Yu-Qin Yuan, Dong-Li Fan

Key Laboratory of Systems Bioengineering, Ministry of Education, School of Chemical Engineering and Technology, Tianjin University, Tianjin 300072, China

ARTICLE INFO

Article history:
Received 25 September 2013
Received in revised form 11 December 2013
Accepted 23 December 2013
Available online 31 December 2013

Keywords:
Pyrazinecarboxamide
Self-assemble
Organogelator
Stimuli responsive
Mesophase

ABSTRACT

A series of new low molecular organogelators (LMOGs) with thermotropic mesophase were synthesized via the reaction of 3,6-dimethyl-pyrazine-2,5-dicarboxylic acid with *p*-alkoxyl anilines. These compounds readily formed stable gels in a variety of organic solvents and their self-assembly behavior, structure–property relationship were investigated by scanning electron microscopy (SEM), X-ray diffraction (XRD), ^{1}H nuclear magnetic resonance (^{1}H NMR), Fourier transform infrared spectroscopy (FTIR) and ultra-violet–visible spectroscopy (UV). The results showed a combination of intra-hydrogen bonding, π–π stacking and van der Waals interaction resulted in the aggregation of the organogelators to form three-dimension fibrous networks. The gels formed were multi-responsive to environmental stimuli, such as temperature, fluorinion, and shear stress. More importantly, all the organogelators exhibited thermotropic hexagonal column mesophase as revealed by differential scanning calorimetry (DSC), polarized optical microscopy (POM), and variable temperature XRD studies. A control compound was synthesized and its gelling ability was also checked.

1. Introduction

Low molecular organogelators (LMOGs) self-assemble to form organogels via noncovalent interactions, such as hydrogen bonding, π–π stacking, van der Waals interaction, or dipole–dipole interaction, into three-dimensional networks to immobilize the solvent molecules. Liquid crystals (LC) share both the ordered structure of a crystal phase and the molecular mobility of an isotropic (liquid) phase. Among various soft materials, supramolecular gels and liquid crystalline materials are of great interest ones not only because they can generate one dimensional stacks of functional molecules through molecular self-assembly without using advanced techniques but also they can respond to a wide range of external stimuli, such as temperature, electrical pulse, light, shearing, and chemicals.[1] In recent years, intensive research has paid to the development of new functional organogels and liquid crystalline materials.[2] The motivation to study these supramolecular organizations of various functions results from the desire to control precisely over their interactions and resulting various chemical–physical properties, which are highly relevant and desirable in their practical utility. In order to make use efficiently of LC in electronic devices, great effort has been made to address properties, such as ferroelectricity, electrical or photoconductivity, light emission, or information storage.[3] The linear structure resulting from the self-assembly of π-conjugated molecules is specially emphasized in preparing soft materials for their potential applications in photonics and optoelectronics.[4,3b]

The relationship between gelation and mesophase is subtle. To achieve gelation, a balance between the tendency of the gelator molecules to dissolve or to aggregate is essential while a balance between the tendency of the molecules to melt or to microsegregate into a noncrystalline state is required for the mesomorphic state. Usually, it is difficult to expect the balance between the tendency of the molecules to dissolve/melt and to aggregate. As a result, low molecular weight compounds having both the gelling ability and displaying thermotropic mesomorphic behavior at the same time remain relatively rare,[5] indicating it is really serendipity to obtain low molecular compounds capable of gelling solvents and exhibiting thermotropic mesomorphic behavior.

Pyrazine dicarboxylic acids, as well as their simple carboxylates and amides, can act as multidentate ligands and have been proven to be elegant ligands in crystal engineering. The use of them as parent molecules for the construction of binuclear or polynuclear complexes is well established and documented.[6] However, little attention has been paid to the gel and/or LC properties of pyrazine

* Corresponding author. Fax: +86 22 27890166; e-mail addresses: huangyaodong@tju.edu.cn, hyd224@tju.edu.cn (Y.-D. Huang).

0040-4020/$ – see front matter © 2013 Elsevier Ltd. All rights reserved.
http://dx.doi.org/10.1016/j.tet.2013.12.060

dicarboxylic acid derivatives though a quasi-pyrazine dicarboxylic acid derivative (hexaazatriphenylene hexacarboxylic acid) has been reported involving in the synthesis of an electron-deficient liquid crystalline material.[7] Here in, we would like to present the synthesis and combined features of both gel and LC of a series of pyrazine diamide derivatives.

2. Results and discussion

2.1. Synthesis

The synthetic route of pyrazinecarboxamide derivatives was shown in Scheme 1. *p*-Alkoxyl anilines **3** were prepared according to the literature[8] and 3,6-dimethyl-pyrazine-2,5-dicarboxylic acid **5** was obtained by the oxidation of **4** with potassium hypermanganate. Compound **6** was obtained after overnight's reflux of **5** with thionyl chloride ($SOCl_2$) following the evaporation of residual $SOCl_2$ under reduced pressure and it was used directly without any purification. The general procedure for the preparation of compounds **7** was as followings. Under nitrogen atmosphere, *p*-alkoxyl aniline **3** (2.5 mmol), anhydrous triethyl amine (6 mmol) and 20 mL chloroform were mixed in a flask and then cooled to 0 °C. The chloroform solution of **6** (1 mmol) was added dropwise to the stirring solution and the mixture was stirred for 3 h at room temperature. The solids were collected by filtration and washed with ethanol. The product was isolated by column chromatography on silica gel using dichloromethane and petroleum ether (8/1, v/v) as eluent to give a yellow solid at the yield about 40%. Control compound **8** was obtained via the reaction of **6** with *n*-dodecyl amine.

Table 1
Gelation properties of 3,6-dimethyl-2,5-pyrazine diamide derivatives **7a**–**f** and **8**[a,b]

Solvent	7a	7b	7c	7d	7e	7f	8
Dichloromethane	50	50	25	25	25	20	65
Chloroform	S	S	PG	50	25	16	P
Tetrachloromethane	P	PG	PG	PG	PG	PG	35
Acetone	P	P	Ins	Ins	Ins	Ins	Ins
Diethyl ether	P	P	Ins	Ins	Ins	Ins	Ins
Ethyl acetate	P	PG	50	50	33	33	57
THF	PG	PG	25	20	20	16	25
DMF	PG	PG	50	10	10	8	20
Benzene	PG	PG	50	50	25	25	56
Toluene	PG	PG	50	50	25	25	53
Dimethylbenzene	P	P	P	P	P	P	26
Chlorobenzene	33	33	25	25	20	20	38
Methanol	Ins	Ins	Ins	Ins	Ins	Ins	Ins
Ethanol	Ins	Ins	Ins	Ins	Ins	Ins	Ins
Isopropanol	Ins	Ins	Ins	Ins	Ins	Ins	Ins
Hexyl alcohol	Ins	Ins	Ins	Ins	Ins	Ins	Ins
DCE	25	25	25	20	16	14	34
Dioxane	50	50	25	20	10	8	22
Hexane	Ins	Ins	Ins	Ins	Ins	Ins	Ins
Petroleum ether	Ins	Ins	Ins	Ins	Ins	Ins	Ins
Pyridine	PG	PG	50	20	10	8	32
Acetonitrile	Ins	Ins	Ins	Ins	Ins	Ins	Ins
Triethylamine	Ins	Ins	Ins	Ins	Ins	Ins	Ins
Aniline	PG	50	50	25	20	20	28
Carbon disulfide	P	50	50	25	20	16	31
DMSO	33	33	20	10	7	5	20
Water+DMSO(1/4)	P	P	PG	PG	PG	PG	P
Water+DMSO(1/1)	P	P	P	PG	PG	PG	P
Water+DMSO(4/1)	P	P	P	P	P	P	Ins

[a] Values denote the minimum gel concentration (GMC, mg/mL) to achieve gelation at room temperature. S: solution; PG: partial gel; Ins: insoluble; P: precipitation.
[b] THF, DMF, DCE, and DMSO indicate tetrahydrofuran, *N*,*N*-dimethylformamide, 1,2-dichloroethane, and dimethyl sulfoxide.

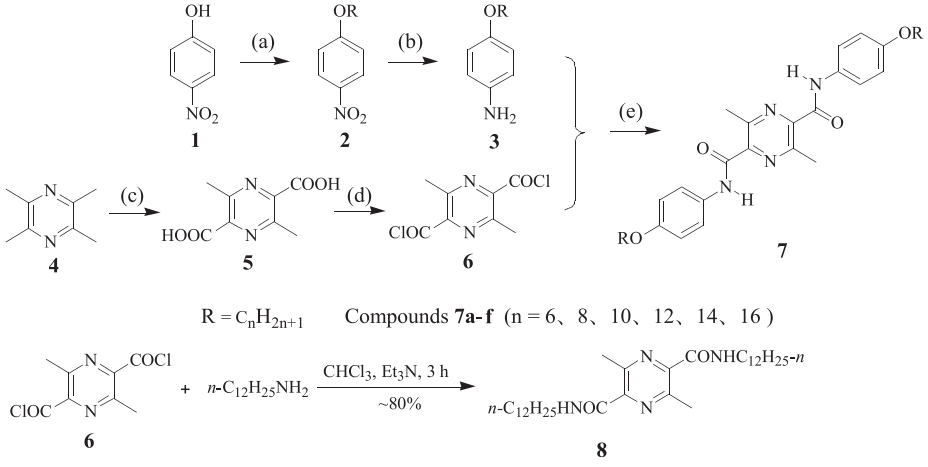

(a) RBr, DMF, K_2CO_3, 70–80 °C, 5 h, ~96%; (b) $NH_2NH_2{\cdot}H_2O$, C_2H_5OH, graphite, reflux, 48 h, ~90%; (c) $KMnO_4$, H_2O, reflux, 4 h, ~50%; (d) $SOCl_2$, reflux, overnight, ~99%; (e) $CHCl_3$, Et_3N, 3 h, ~40%.

Scheme 1. Synthetic route for gelators **7a**–**f** and control compound **8**.

2.2. Gelation properties

The gelation behaviors of compounds **7a**–**f** and **8** were tested for different solvents including protic/aprotic and polar/apolar solvents at room temperature and the results are summarized in Table 1.

As shown in Table 1, all the six compounds **7a**–**f** cannot dissolve in either high polar solvents, such as alcohols or apolar alkanes, such as petroleum ether and hexane. Compounds **7c**–**f** can gel some chloro-aliphatic solvents (dichloromethane, DCE), amines (aniline, DMF), aromatic solvents (benzene, toluene, chlorobenzene and pyridine) while **7a** and **7b** only give partial gels. A careful examination of minimum concentration values reveals that the length of the aliphatic chains plays a crucial role in the gelating ability of the gelator. The compound with longer side chains gelate broader range of solvents with lower MGC than that with shorter side chains, which results from a hydrophobic–hydrophilic balance of the molecule, i.e., the balance of polar hydrogen bonding units and non-polar alkyl chains.[9] Although compounds **7a**–**f** are insoluble in water, some of them can

form partial gels in aqueous DMSO and obviously longer alkyl chains help the gelator forms partial gel in a lower concentration of DMSO (**7c**–**f** in water/DMSO=1/4, **7d**–**f** in water/DMSO=1/1). In addition, the sol-gel transition is well thermoreversible even after many cycles of heating-cooling and the organogels are found to be stable for months at room temperature. As a control compound, **8** does not have two phenyl rings, meaning it lacks the π–π interaction of phenyl rings. As a result, **8** is an inferior gelator comparing to its counter **7d**, though it has better performance in case of tetrachloromethane and dimethylbenzene. The observations imply the π–π interaction is a driving force of gelation for **7a**–**f**.

To examine the gels thermostabilities, the gel–sol phase transition temperatures (T_{gel}) of **7d** and **7f** at different concentrations in dioxane, pyridine, and 1,2-dichlorlethane were determined, respectively, by using a tube-inversion methodology.[10] Fig. 1 shows the checking results. Similar to the reported in literature,[11] all the T_{gel} increased with the increasing of gelator concentration, indicating higher stability of the gel networks in higher concentrations. It also should be noted that under the same solvent and concentration, the T_{gel} of **7f** was higher than that of **7d**, suggesting longer side chains in the gelator formed a stronger gel network. Among the solvents, the T_{gel} values appear in the order of dioxane>pyridine>1,2-dichloroethane.

2.3. Morphology and XRD study

In order to obtain a macroscopic aspect of the network structures of the gels, the xerogels of compounds **7c**–**f** from benzene, dichloromethane, dioxane, and THF were subjected to SEM. The xerogels were obtained after drying the selected gels in the atmosphere for 72 h. It is reported a gel formed at first and then collapsed into a crystal after a certain time at room temperature,[12] however, in the case of **7a**–**f**, such collapse does not occur. In the experiment, the xerogels from air-dried had almost the same SEM images with that from freeze-dried samples except the ribbons of the latter were a little wizened than that the former ones. As shown in Fig. 2, most xerogels of **7c** and **7f** exhibited well-defined fibrous-type ribbons with the width of 0.1–2 μm, which entangle to 3D cross-linking network. The xerogels of **7d** and **7e** also had the similar morphology (not shown). The only exception of them is the xerogel of **7f**/dioxane (Fig. 2G), which showed much regular structure with many quadrate or trapeziform holes. It seems this unique fishnet structure can help to improve the gelating efficiency since its MGC is the lowest one (Table 1). Apparently, the morphologies of these xerogels are somewhat independent of the gelator and gelating solvents although there are differences in fine structures.

X-ray diffraction (XRD) technique was used to investigate the structures of xerogels. Thick films of the dried gels from dioxane or

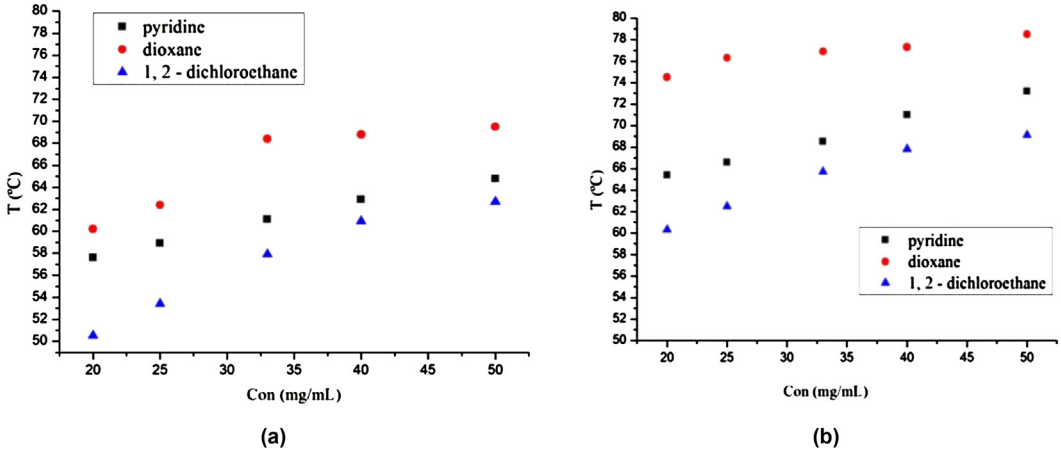

Fig. 1. Plots of T_{gel} against the concentration of (a) **7d** and (b) **7f** in pyridine, dioxane, and 1,2-dichloroethane with the heating rate 2 °C/min in water bath.

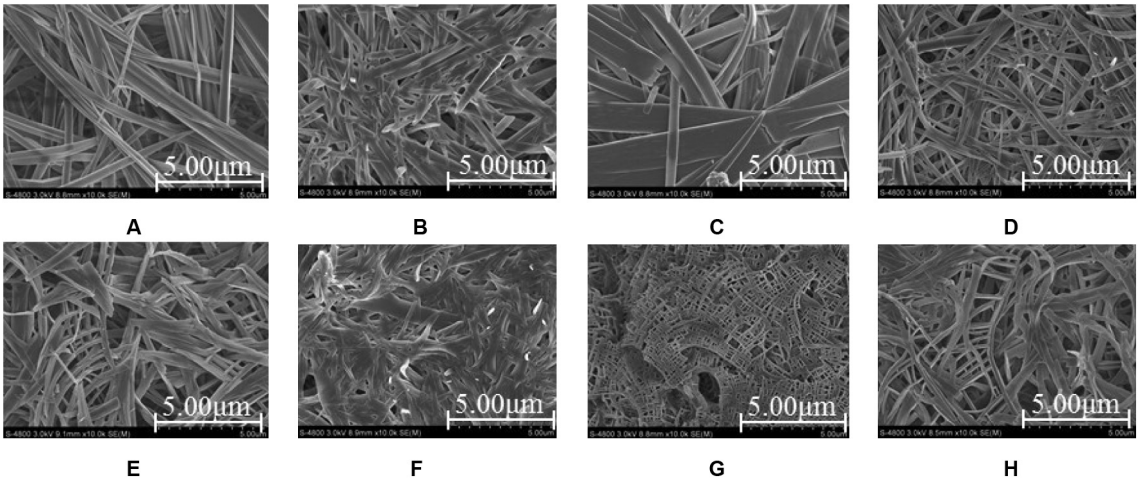

Fig. 2. SEM images of the xerogels from the gels of (A) **7c**/benzene, (B) **7c**/dichloromethane, (C) **7c**/dioxane, (D) **7c**/THF, (E) **7f**/benzene, (F) **7f**/dichloromethane, (G) **7f**/dioxane, (H) **7f**/THF.

dichloromethane were prepared on glass plates and their X-ray diffractograms were recorded on a Bruker diffractometer using Ni filtered Cu Kα radiation. The resulting spectrum of the xerogel obtained from **7f** in dioxane is shown in Fig. 3. The long spacing *d* values of the aggregate are 29.0, 14.5, 9.7, and 7.2 Å, which are almost exactly 1:1/2:1/3:1/4, indicating a lamellar packing of the gelator. Similar XRD were performed on the xerogels of **7a**–**e** from dioxane and **7f** from dichloromethane and the results are also listed in Table 2. As shown in Table 2, all the spacing values of them have a reciprocal ratio of 1:1/2:1/3:1/4, suggesting all the gelator molecules aggregate to a lamellar structure. The interlayer distances of xerogels of **7a**–**f** from dioxane are 18.5, 20.1, 22.0, 24.4, 26.6, and 29.0 Å, respectively, increasing expectedly with the length increase of the side chains. Though a great difference is found between the morphologies of xerogels of **7f** from dichloromethane and **7f** from dioxane (Fig. 2F and G), they have almost the same interlayer distances around 29.0 Å.

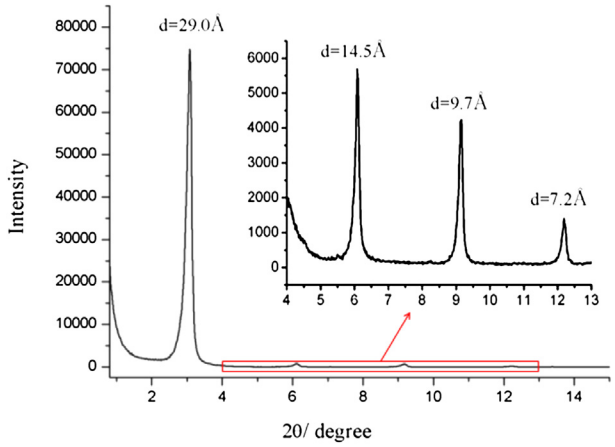

Fig. 3. XRD pattern of the xerogel from **7f** in dioxane.

Table 2
Bragg reflections observed in xerogels of **7a**–**f**

Compound	Solvent	d_{100} (Å)	d_{200} (Å)	d_{300} (Å)	d_{400} (Å)
7a	Dioxane	18.5	9.2	6.2	4.6
7b	Dioxane	20.1	9.5	7.1	5.4
7c	Dioxane	22.0	11.1	7.3	5.5
7d	Dioxane	24.4	12.2	8.1	6.1
7e	Dioxane	26.6	13.3	8.9	6.7
7f	Dioxane	29.0	14.5	9.7	7.2
7f	Dichloromethane	28.9	14.5	9.6	7.2

Fig. 4 shows the wide angle X-ray diffraction (WAXD) of the **7f** xerogel from dioxane. The observation of a peak at 2θ=19.7° with *d* space 4.5 Å implies the liquid-like arrangement of the alky chains in the gel is well ordered.[5e,13] The peak at 2*θ*=23.9° with *d* space 3.7 Å connects to the existence of strong π–π interactions in the gel.[14,1c] Obviously, the π-π interactions and van der Waals interactions are the driving forces of gelation.

2.4. Spectroscopic study

2.4.1. FTIR study. To elucidate the driving forces for the organogelation, FTIR spectra were measured. Fig. 5 shows the FTIR spectra of **7f** at different states. It can be seen that the spectrum of xerogel of **7f** obtained from dioxane (Fig. 5c) is very similar to that of the crystal from $CHCl_3$ (Fig. 5b), indicating the two forms of **7b** exist the same noncovalent interactions.

As shown in Fig. 5a and c, the absorption bands of amide N–H and C=O shifted from 3362 cm^{-1}, 1681 cm^{-1} in the $CHCl_3$ solution

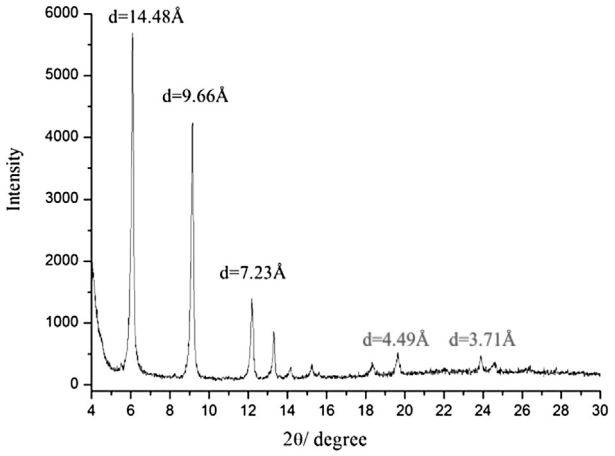

Fig. 4. Wide angle X-ray diffraction of the xerogel of **7f** obtained from dioxane.

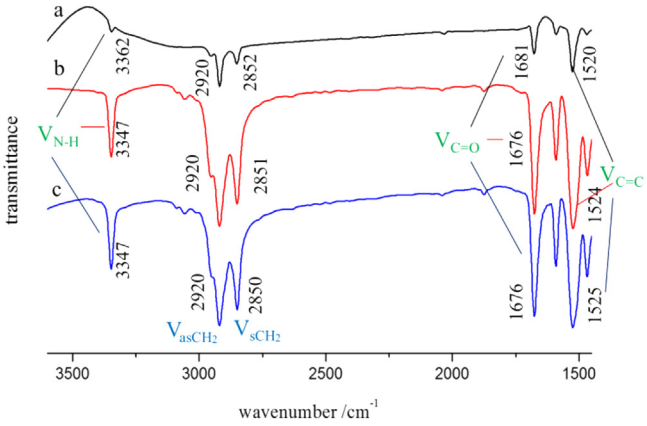

Fig. 5. FTIR spectra of **7f**: (a) $CHCl_3$ solution, (b) the crystal from $CHCl_3$, and (c) the xerogel from dioxane.

to 3347 cm^{-1}, 1676 cm^{-1} in the dioxane xerogel. The red-shifts of the amide N–H stretching vibration (15 cm^{-1}) and C=O stretching vibration (5 cm^{-1}) demonstrated the presence of hydrogen bonding between the amide groups in the gel state. It should be noted that in Fig. 5a, hydrogen bonded N–H stretching peak were observed at 3362 cm^{-1}, but no peaks were found in free N–H stretching region (3400–3500 cm^{-1}). This phenomenon means the hydrogen bonding is intramolecular rather than intermolecular.

2.4.2. UV study. It has been reported UV–visible spectroscopy is a useful tool to discriminate the *H*-aggregation and *J*-aggregation.[15] Fig. 6 shows the UV–visible spectra of **7f** in solution and gel state. The three absorption peaks at 234, 276, and 364 nm in the sol phase shift to longer wavelength up to 252, 296, and 422 nm in the gel phase, respectively. This red shift indicates the formation of *J*-aggregate in the gel, which is also a reflection of new motif of hydrogen bonding and π–π interaction involving in the formation of the gel network.

2.4.3. ^1H NMR study. To further depict the motif of hydrogen bondings, temperature-dependent ^1H NMR spectra of **7f** in $CDCl_3$ were performed. As shown in Fig. 7a, at low temperature of 298 K, broad and weak proton signals were observed due to the extensive aggregation of **7f** in gel state. With the increasing temperature from 298 K to 328 K, all of the signals in the spectra became sharp and strong, along with the upfield shift of amide proton's signal. The shift resulted from the gradual breakdown of the hydrogen bonding

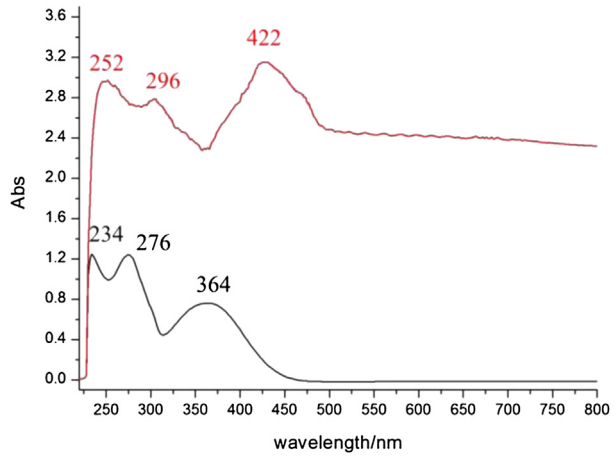

Fig. 6. UV–visible absorption of **7f** in the gel state (chloroform, 20 mg/mL) (red line) and in the solution state (chloroform, 6.05×10^{-4} M) (black line).

the aromatic protons are found to shift slightly to lower field with the increase of temperature, revealing the gradually weakening of the π–π stacking interaction with the gradually collapse of gel network. As can be seen from Fig. 7b, the two doublet signal resonances from phenyl rings upfield shift slightly when the concentration increase. The results of ^{1}H NMR indicate obviously the π–π stacking interaction is involved in the formation of gel.

2.5. Stimuli response study

Some organogels with hydrogen bondings are reported to liable to reach reversible gel–sol–gel transition by adding and removing some anions.[17] To examine the anion binding properties of the 3,6-dimethyl-2,5-pyrazine diamide derivatives, the DMF gel of **7c** was chosen as a sample. After the addition of five kinds of anions (F^-, Cl^-, Br^-, I^-, and AcO^-, as n-Bu_4N^+ salt), respectively, four gels remained unchanged (Fig. 8a) while the gel with 1.5 equiv of F^- collapsed (Fig. 8b). This is because the addition of F^{-1} will result in

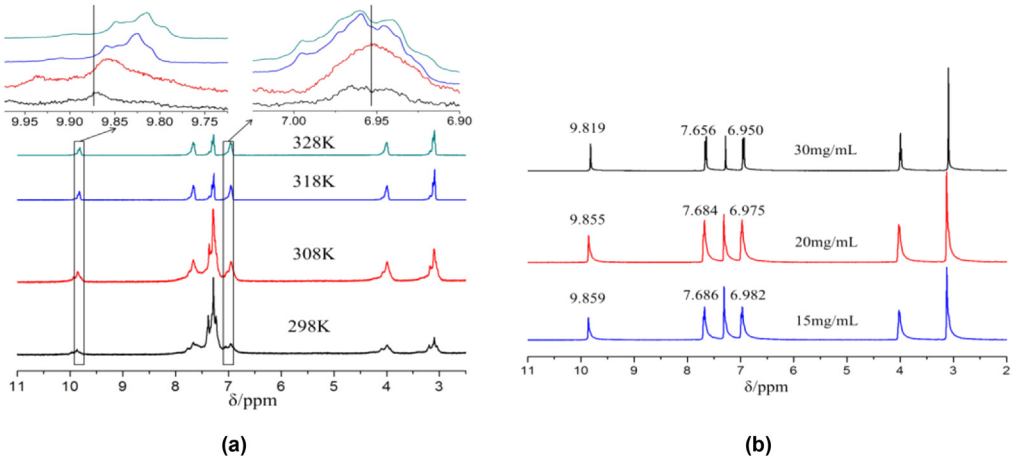

Fig. 7. (a) Temperature-dependent ^{1}H NMR spectra of **7f** in $CDCl_3$ (20 mg/mL); (b) concentration-dependent ^{1}H NMR spectra of **7f** in $CDCl_3$ (318 K).

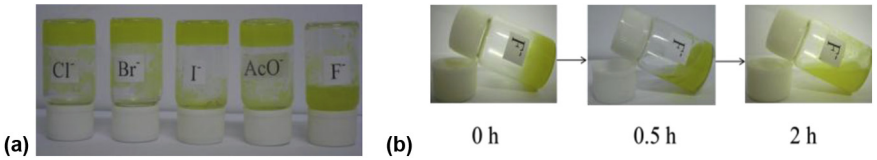

Fig. 8. State changes of the DMF gel of **7c** (50 mg/mL) in anion response test: (a) responses to different anions, and (b) the collapse of the gel with F^-.

network at elevated temperatures. According to the literature,[16] internally hydrogen bonded amides show a much smaller shift with temperature ($<3.0\times10^{-3}$ ppm K^{-1}) compared to those directed externally and accessible for hydrogen bonding to a polar solvent ($>4.0\times10^{-3}$ ppm K^{-1}). The amide–NH groups of **7f** give a small upfield shift with the temperature (2.0×10^{-3} ppm K^{-1}) in $CDCl_3$, which indicate the existence of intramolecular hydrogen bonding rather than intermolecular hydrogen bonding. In order to verify this point, the concentration-dependent ^{1}H NMR measurement of **7f** in $CDCl_3$ was conducted. To avoid the formation of gel, the measurement was done at 318 K and the results were shown in Fig. 7b. The chemical shifts of the NH protons only had a little increase (0.04 ppm) with the increasing of concentration from 15 mg/mL to 30 mg/mL, implying they do form intramolecular hydrogen bonding. This conclusion is consistent with the result obtained from IR spectrum. As contrast to the upfield shift of amide protons, the formation of F···HNCO hydrogen bonding and destroy the original N···HNCO intramolecular hydrogen bonding. The collapsed 'gel' can be revived by the adding of Ag^+, or a protic solvent, such as CH_3OH. It is reasonable to deduce the addition of CH_3OH to the collapsed 'gel' will break the F···HNCO hydrogen bonding and reform the N···HNCO intramolecular hydrogen bonding. In case of the using of Ag^+, it will yield a black rather than yellow gel because of the formation of AgF and the reaction of AgF with moist air. The gel–sol and sol–gel transitions result from the destruction/formation of hydrogen bonding network and it is clearly the intramolecular hydrogen bonding of the HNCO group is the major driving force for gelation. The result of ^{1}H NMR titration shown in Fig. 9 manifests the formation of hydrogen bonding between F^- from *tetra-n*-butylammonium fluoride (TBAF) and reactive amide protons, which will destroy the intra-hydrogen bonding in molecules of **7c**.

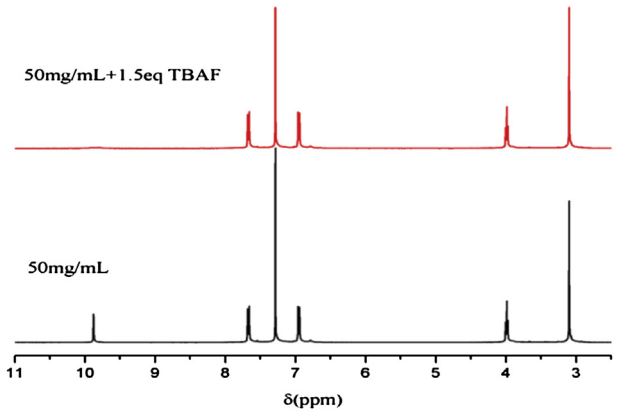

Fig. 9. ^{1}H NMR spectra of **7c** in $CDCl_3$ with and without F^-.

Aside from the response to F^-, the organogels were found to exhibit thixotropic behavior. The imposition of the mechanical or sonic stimuli on the gels could cause the ruin of them, which could turn to gels again after resting for 18–24 h. For example, shaking or sonicating the dioxane gel of **7f** for 2 min will turn the gel into free-flowing liquid, which take about 18 h to re-form the gel (Fig. 10). It is interesting that Cu(II) salts, such as $CuCl_2$ can accelerate the re-formation of gel. Furthermore, the degree of acceleration depends on the amount of Cu(II) salt. In the case of **7f** in dioxane, the re-formation time was 8 h when the vial contained 2 equiv $CuCl_2$ and the time reduced to 3 h when the vial contained 4 equiv of metal salt. Considering simple amides of pyrazine dicarboxylic acids are efficient ligands, the acceleration ability of Cu(II) maybe results from the formation of coordination bond between Cu(II) and N atom in pyrazine ring, which facilitates the recovery of the extended π–π interactions of the system.

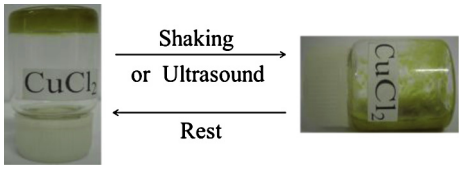

Fig. 10. The mechano or ultrasound responsive test of **7f**.

2.6. Mesophase properties of the gelators

As revealed in above-mention, all the synthesized compounds **7a**–**f** are efficient organogelators and their xerogels show pretty good WXRD patterns with sharp peaks, indicating they possess highly ordered structures and the possibility of having mesophase. In order to check the thermal behaviors of **7a**–**f**, they were subjected to POM, DSC, and variable temperature XRD. To our surprise, all the six compounds cannot only act as efficient organogelators but also self-organize into thermotropic liquid crystals.

2.6.1. Polarized optical microscopy (POM). Under the observation of POM, all the six investigated compounds exhibited fluid and homogeneous textures characteristic of columnar mesophases. Fig. 11 gives POM images of **7a**–**f** taken upon cooling from their isotropic state. Usually, the increase of the length of substituted side chains will depress the melting temperature. The clearing points of the compounds varies from 183 °C for **7a**, bearing the shortest alkoxy chains, to 138 °C for **7f**, containing the longest alkoxy chains. Obviously, the clearing point is correlated with the length of side chains, although the decrease seems to almost saturate after the length gets longer than that in **7e**, where the temperature is almost the same of the **7f** (139 °C and 138 °C, respectively). The length of alkoxy chains also has great influence on the mesomorphic temperature domain, which is found to be 11, 12, 11, 11, 6, and 2 °C for **7a**–**f**, respectively. The control compound **8** was also subjected to POM study, however, it melted directly into isotropic liquid at 128 °C and did not show any birefringent texture on the cooling from isotropic liquid to room temperature. Considering the structural difference between **7d** and **8**, a conclusion can be drawn that the lack of π–π interaction among phenyl rings results in the loss of mesophase. That is to say, π–π interaction plays a crucial role in the forming of liquid crystal.

2.6.2. Differential scanning calorimetry (DSC). The thermal behavior of these new pyrazine diamide derivatives was further investigated by DSC. All the DSC experiments were made under a nitrogen atmosphere with heating and/or cooling rates of 10 °C/min. Fig. 12 shows the thermal behavior of **7d**. When cooled from the isotropic liquid state to room temperature, **7d** exhibits a small exotherm at 139.0 °C with a ΔH of 6.8 kJ/mol, corresponding to the transition from the isotropic liquid to the liquid crystalline phase. In the POM study, pseudo-fan-shaped texture appears at 144.1 °C in

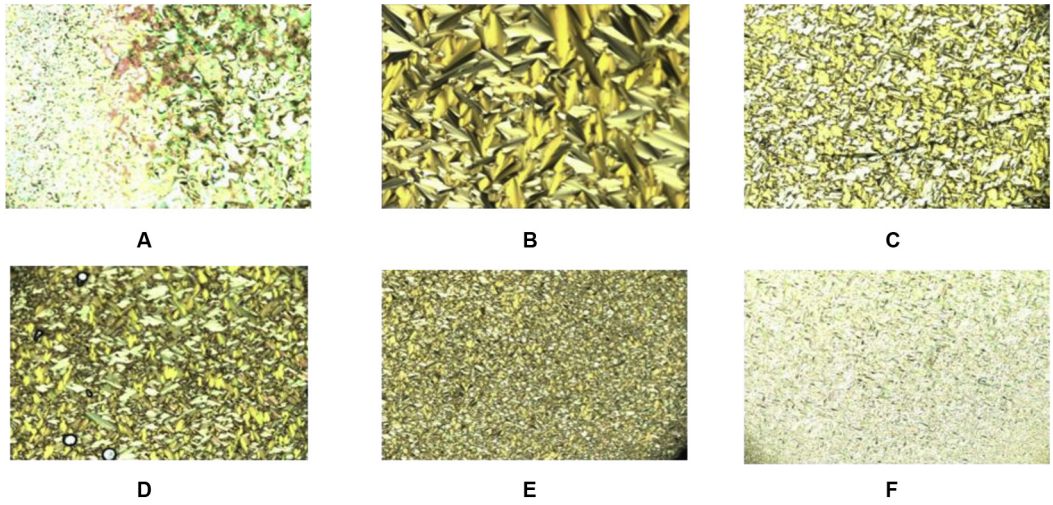

Fig. 11. POM images of **7a**–**f** taken upon cooling from their isotropic state. A: **7a** at 150 °C; B: **7b** at 143 °C; C: **7c** at 140 °C; D: **7d** at 140 °C (the circles are air bubbles); E: **7e** at 137 °C; F: **7f** at 133 °C. (Magnification: ×200).

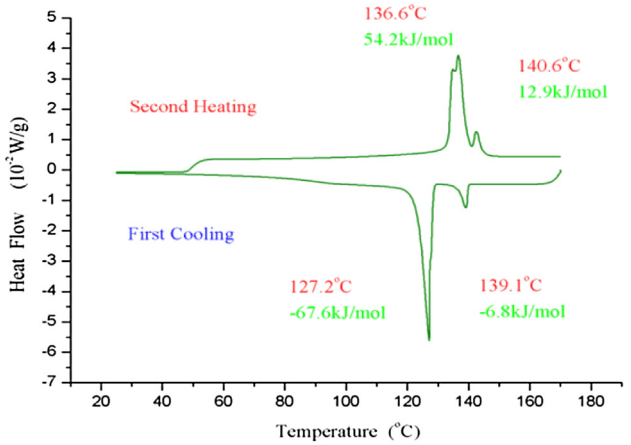

Fig. 12. DSC first cooling run (lower) and second heating run (upper) of compound **7d**.

the first cooling run. In the second DSC heating run, compound **7d** exhibits an endotherm at 140.6 °C with a Δ*H* of 12.9 kJ/mol, corresponding to the transition from the liquid crystalline phase to the isotropic liquid. The DSC results of all compounds are summarized in Table 3. As shown in Table 3, the behavior of the pyrazine diamide compounds is quite different. Very narrow mesophase transitions are found for **7b**, **7c**, **7d**, and **7e** while no clues of mesophase are given for **7a** and **7f** by DSC. As a result, the existence of mesophase in **7a** and **7f** can only be confirmed by POM and variable temperature XRD. Similar observations are also found in literature.[18] Considering the longer side chains of **7a**–**f** always having a positive trend in gelating ability, it is interesting to observe the irregular role it plays on the thermotropic mesomorphic phase of these gelators.

Table 3
DSC characterization of the pyrazine diamide derivatives under first cooling run.[a]

Compound	Transition	Temperature (°C)	Δ*H* (kJ mol^{-1})	Mesophase width (°C)
7a	I→(Col$_h$)[b]→Cr	140	−42.6	11[c]
7b	I→Col$_h$	142	−4.15	7
	Col$_h$→g	135	−33.0	
	g→Cr	114	−21.0	
7c	I→Col$_h$	141	−4.9	8
	Col$_h$→g	133	−27.9	
	g→Cr	124	−17.0	
7d	I→Col$_h$	139	−6.8	12
	Col$_h$→Cr	127	−67.6	
7e	I→Col$_h$	133	−0.68	2
	Col$_h$→Cr	131	−70.5	
7f	I→(Col$_h$)[b]→Cr	131	−103.9	2[c]

[a] Cr=crystal; Col$_h$=hexagonal columnar mesophase; I=isotropic phase; g=glassy state.
[b] The phase transition cannot be detected by DSC and it is confirmed by POM and variable temperature XRD.
[c] The value comes from the changes of the texture observed in POM.

2.6.3. Variable temperature XRD. Variable temperature X-ray diffraction was performed on these pyrazine diamide derivatives to get further information on molecular arrangements in their mesophases. Because compounds **7e** and **7f** have a very narrow liquid crystalline phase interval, the detections on them fail to give useful information. Fig. 13 shows the XRD patterns of **7a** at 148 °C.

Though the DSC pattern of **7a** does not show unambiguously information about LC, its XRD thermogram gives two peaks with *d* spacings of 22.6 and 12.6 Å, respectively, in low angle region. The two *d* spacings are in the ratio of 1:1/√3 and readily assigned as (100) and (110) reflections of the hexagonal lattice with a parameter *a*=26.1 Å. In wide angle region, a strong and diffuse broad halo with maximum at about 4.5 Å and a sharp peak with a maximum at

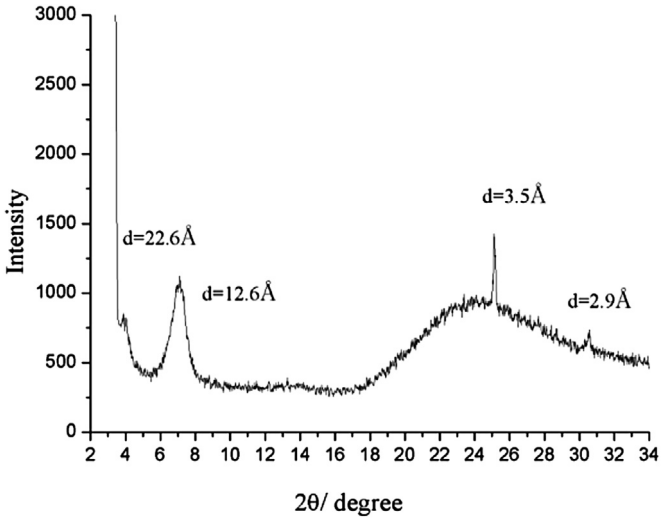

Fig. 13. X-ray diffraction pattern of **7a** at 148 °C.

3.5 Å indicate the molten aliphatic chains in liquid-like conformation and a strong intermolecular π–π stacking, respectively, involving in the formation of hexagonal columnar structure.[19] It is also worthy to be noted a medium strong peak appears at 2θ=30.5°, with *d*=2.9 Å, which is supposed to correspond to the distance between pyrazine rings of the adjacent molecules. The results of XRD are in good agreement with that of POM, revealing the existence of hexagonal columnar mesophase. The detections of **7b**, **7c**, and **7d** give highly similar XRD thermograms with that of **7a** and their diffraction data are listed in Table 4. The interlayer distances of **7a**, **7b**, **7c**, **7d** are 22.6, 22.8, 22.9, and 23.1 Å, respectively, only increasing slightly with the length increase of the side chains.

Table 4
Variable temperature X-ray diffraction data for compounds **7a**–**d**

Compound	d_{100} (Å)	d_{110} (Å)	π–π stacking (Å)	*a* (Å)[a]
7a	22.6	12.6	3.5	26.1
7b	22.8	12.6	3.5	26.3
7c	22.9	12.6	3.5	26.4
7d	23.1	12.7	3.6	26.7

[a] The lattice parameter, *a*, is defined as $a=2<d_{100}>/\sqrt{3}$.

To gain insight into the secrets of the compounds under mesophase state, the density of them was calculated on the basis of the parameters measured by XRD. It is known the relationship between the density ρ of the compound and the number *Z* of molecules in a unit cell is given by the equation $\rho=(M/N)/(V/Z)$, where *M* is the molecular weight (in g mol^{-1}), *N* the Avogadro number, and *V* the unit cell volume (in cm^3). For the Col$_h$ organization, volume of the hexagonal cell is given by $V=h\times S$, where *h* is the mean stacking distance between the molecular cores along the column (*h* parameter of the Col$_h$ mesophase), *S* the columnar cross-sectional area, which is given by $S=a\times d_{10}$ (*a* is the lattice parameter and d_{10} the *d* spacing of (100) reflection). The calculating density ρ are 0.44*Z*, 0.48*Z*, 0.52*Z*, 0.53*Z* for **7a**, **7b**, **7c**, **7d**, respectively. Since the density values of organic mesomorphic materials must be close to 1 g cm^{-3}, *Z* must have a value of 2. That is to say, each column slice (or hexagonal network node) contains two molecules of compound **7a**, **7b**, **7c** or **7d**. Taken as an example, the geometry of single **7d** molecule was simulated by SYBYL 6.92 simulation software using the PM3 method. As shown in Fig. 14, the pyrazine ring and two OCNH groups are coplanar arrangement while two aryl rings adopt

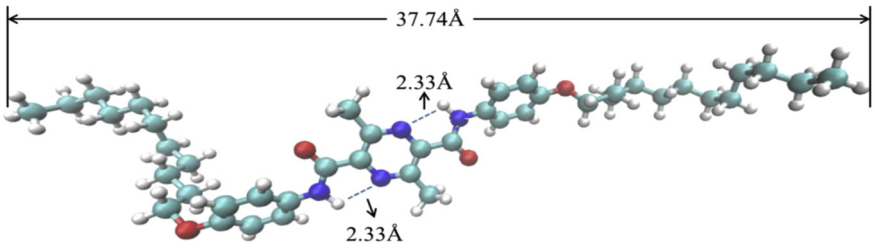

Fig. 14. A molecular mode of **7d** showing different structural motifs.

parallel assignment with a vertical distance about 2.8 Å. The coplane of pyrazine ring with two OCNH groups is attributed to the two intra-hydrogen bondings forming by the two protons of amide groups with the two nitrogen atoms of pyrazine ring. Both the two intra-hydrogen bondings have the same length of 2.33 Å. Interestingly, the plane of aryl ring diverges from the pyrazine ring with a dihedron angle of ca. 56.5°. Under fully extended conformation of its alkyl chains, the molecular length of **7d** is 37.7 Å (Fig. 14). The value is much bigger than the lattice parameter of the Col_h phase of **7d**, where a=26.7 Å. This difference stems from the shrinkage of alkyl chains in the Col_h LC phase rather than the conformation changing of the core structure, i.e., the pyrazine ring and two aromatic rings adopting a *trans*-conformation with no intramolecular hydrogen bonding. The intramolecular hydrogen bonding in the compound is strong and it helps to maintain the coplane of pyrazine ring with two OCNH groups. The adoption of such *trans*-conformation will result in the disappearance of intramolecular hydrogen bonding and the twist of the molecule, which lead to higher energy and less stability. Moreover, a twist structure will destroy the π–π stacking, an important driving force for the molecules self-assembling into long-range ordered columnar structure and finally showing mesophase. That is to say, the existence of the mesophase indicates the core structure of compound does not adopt *trans*-conformation. As to the shrinkage of alkyl chains in the Col_h LC phase, it is also reported in literature.[20]

3. Conclusion

In summary, a new series of pyrazine carboxamides have been prepared and their gelation ability, supramolecular architectures, and liquid crystal properties have been investigated. All the compounds are efficient organogelators and exhibit thermotropic mesophase. The organogels show multistimuli responsive behaviors and the driving forces of gelation are intra-hydrogen bondings, π–π stacking interactions and van der Waals interactions. The length of the aliphatic chains has great influence not only on gelating ability but also on thermal behavior. Longer alkyl chains facilitate to promote the gelation efficiency of the gelator while exhibit irregular influence on their mesomorphic temperature domain. The strong π–π interactions result in the molecules of gelators self-assembling into long-range ordered columnar structure and finally showing mesophase under the cooperation of van der Waals interactions.

4. Experimental section

4.1. Materials and measurements

All the chemicals were purchased from commercial chemical suppliers and used without further purification. ^{1}H nuclear magnetic resonance (^{1}H NMR) spectra were recorded with a Bruker 400 spectrometer operated at 300 MHz and ^{13}C nuclear magnetic resonance (^{13}C NMR) spectra were recorded with a Bruker 400 spectrometer operated at 100 MHz. Accurate mass data were obtained with an Agilent Technologies 6520 Accurate-Mass Q-TOF LC/MS instrument and a LCQ Advantage MAX instrument, respectively, under ESI model. Fourier transform infrared spectroscopy (FTIR) measurements were performed on a Bio-Rad FTS 6000 spectrometer. Ultra-violet–visible spectroscopy (UV) absorption spectra were recorded with a Lambda35 spectrometer. X-ray diffraction (XRD) was checked on a Bruker diffractometer (Cu Kα radiation k=1.54056 Å). Scanning electron microscopy (SEM) images were taken by Hitachi S-4800 microscope. Polarization optical microscopy (POM) was carried out using an Olympus BX51 microscope equipped with a Linkam LTS 350 platinum heating plate connected to a Linkam TMS 94 processor and the photographs were taken with a Fujix Digital camera HC-300Z. Differential scanning calorimetry (DSC) traces were recorded using a Mettler-Toledo DSC1/500 and the samples were placed in an aluminum crucible and analyzed, under a stream of helium and nitrogen, with a heating/cooling rate of 10 °C/min.

4.2. Synthesis of the gelators 7a–f and control compound 8

The synthetic route and description for the compounds of **7a**–**f** and **8** was presented in Section 2.1.

Compound **7a**: Yellow crystalline solid; yield: 38%. ^{1}H NMR (300 MHz, $CDCl_3$, TMS): δ 9.85 (s, 2H, –CONH); 7.65 (d, J=8.8 Hz, 4H, ArH); 6.93 (d, J=8.8 Hz, 4H, ArH′); 3.98 (t, J=6.5 Hz, 4H, $-OCH_2$); 3.08 (t, J=6.6 Hz, 6H, pyrazine–CH_3); 1.88–1.28 (m, 16H, CH_2); 0.91 (m, 6H, $-O(CH_2)_5CH_3$). ^{13}C NMR (100 MHz, $CDCl_3$): δ 161.16, 156.27, 150.75, 142.81, 130.42, 121.47, 114.84, 68.29, 31.61, 29.26, 26.11, 23.37, 22.62, 14.05. HRMS: calculated for $[M+H]^+$ $C_{32}H_{43}N_4O_4$ 547.3284, found 547.3285.

Compound **7b**: Yellow crystalline solid; yield: 39%. ^{1}H NMR (300 MHz, $CDCl_3$, TMS): δ 9.85 (s, 2H, –CONH); 7.64 (d, J=8.8 Hz, 4H, ArH); 6.94 (d, J=8.8 Hz, 4H, ArH′); 3.98 (t, J=6.5 Hz, 4H, $-OCH_2$); 3.10 (t, J=6.6 Hz, 6H, pyrazine–CH_3); 1.88–1.28 (m, 24H, CH_2); 0.91 (m, 6H, $-O(CH_2)_5CH_3$). ^{13}C NMR (100 MHz, $CDCl_3$): δ 161.19, 156.25, 150.95, 142.17, 130.63, 121.59, 114.97, 68.42, 31.95, 29.39, 26.18, 23.49, 22.80, 14.25. HRMS: calculated for $[M+H]^+$ $C_{36}H_{51}N_4O_4$ 603.3910, found 603.3907.

Compound **7c**: Yellow crystalline solid; yield: 41%. ^{1}H NMR (300 MHz, $CDCl_3$, TMS): δ 9.88 (s, 2H, –CONH); 7.74 (d, J=8.8 Hz, 4H, ArH); 6.95 (d, J=8.8 Hz, 4H, ArH′); 3.98 (t, J=6.5 Hz, 4H, $-OCH_2$); 3.10 (t, J=6.6 Hz, 6H, pyrazine–CH_3); 1.88–1.28 (m, 32H, CH_2); 0.91 (m, 6H, $-O(CH_2)_5CH_3$). ^{13}C NMR (100 MHz, $CDCl_3$): δ 161.17, 156.30, 150.78, 142.76, 130.42, 121.52, 114.88, 68.31, 31.91, 29.57, 29.34, 26.05, 23.37, 22.70, 14.14. HRMS: calculated for $[M+H]^+$ $C_{40}H_{59}N_4O_4$ 659.4536, found 659.4531.

Compound **7d**: Yellow crystalline solid; yield: 42%. ^{1}H NMR (300 MHz, $CDCl_3$, TMS): δ 9.84 (s, 2H, –CONH); 7.64 (d, J=8.8 Hz, 4H, ArH); 6.93 (d, J=8.8 Hz, 4H, ArH′); 3.97 (t, J=6.5 Hz, 4H, $-OCH_2$); 3.08 (t, J=6.6 Hz, 6H, pyrazine–CH_3); 1.88–1.28 (m, 40H, CH_2); 0.91 (m, 6H, $-O(CH_2)_5CH_3$). ^{13}C NMR (100 MHz, $CDCl_3$): δ 161.18, 156.23, 150.79, 142.85, 130.42, 121.52, 114.88, 68.31, 31.93, 29.60, 29.43,

26.05, 23.37, 22.70, 14.14. HRMS: calculated for $[M+H]^+$ $C_{44}H_{67}N_4O_4$ 715.5162, found 715.5160.

Compound **7e**: Yellow crystalline solid; yield: 45%. ^{1}H NMR (300 MHz, $CDCl_3$, TMS): δ 9.85 (s, 2H, −CONH); 7.74 (d, J=8.8 Hz, 4H, ArH); 6.95 (d, J=8.8 Hz, 4H, ArH′); 3.98 (t, J=6.5 Hz, 4H, $-OCH_2$); 3.10 (t, J=6.6 Hz, 6H, pyrazine−CH_3); 1.88−1.28 (m, 48H, CH_2); 0.91 (m, 6H, $-O(CH_2)_5CH_3$). ^{13}C NMR (100 MHz, $CDCl_3$): δ 161.17, 156.43, 150.66, 142.71, 130.34, 121.53, 114.89, 68.32, 31.94, 29.67, 29.43, 29.30, 26.05, 23.37, 22.70, 14.14. HRMS: calculated for $[M+H]^+$ $C_{48}H_{75}N_4O_4$ 771.5788, found 771.5782.

Compound **7f**: Yellow crystalline solid; yield: 46%. ^{1}H NMR (300 MHz, $CDCl_3$, TMS): δ 9.86 (s, 2H, −CONH); 7.74 (d, J=8.8 Hz, 4H, ArH); 6.95 (d, J=8.8 Hz, 4H, ArH′); 3.98 (t, J=6.5 Hz, 4H, $-OCH_2$); 3.10 (t, J=6.6 Hz, 6H, pyrazine−CH_3); 1.88−1.28 (m, 56H, CH_2); 0.91 (m, 6H, $-O(CH_2)_5CH_3$). ^{13}C NMR (100 MHz, $CDCl_3$): δ 161.18, 156.23, 150.79, 142.85, 130.42, 121.52, 114.88, 68.31, 31.93, 29.60, 29.43, 26.05, 23.37, 22.70, 14.14. HRMS: calculated for $[M+H]^+$ $C_{52}H_{83}N_4O_4$ 827.6414, found 827.6297.

Compound **8**: White solid, mp 128 °C. ^{1}H NMR (300 MHz, $CDCl_3$, TMS): δ 8.05 (s, 2H, −CONH); 3.45 (t, 4H, $-NCH_2$); 2.97 (s, 6H, pyrazine−CH_3); 1.65 (m, 4H, $-CH_2$); 1.37−1.27 (m, 36H, $-CH_2$); 0.88 (t, 6H, $-O(CH_2)_{11}CH_3$). ^{13}C NMR (100 MHz, $CDCl_3$): δ 163.89, 150.10, 142.61, 39.54, 29.64, 29.60, 29.55, 29.35, 29.32, 14.13. HRMS: calculated for $[M+H]^+$ $C_{32}H_{59}N_4O_2$ 531.4638, found 531.4642.

4.3. Gelation test

A weighted gelator was mixed with a certain amount of the solvent in a test tube, and the mixture was heated until the solid was dissolved. The resulting solution was then cooled to room temperature, and termed a gel if no fluid solvent ran down when the test tube was inverted. The addition of certain amount solvent and the heating-cooling process was repeated until gel cannot be formed, and the minimum gelation concentration (MGC) can be calculated.

Acknowledgements

We gratefully acknowledge the financial support from Graduate School of Tianjin University. We also thank National Engineering Research Center of Industrial Crystallization Technology, China (NERCICT) for access to the POM and DSC facilities.

Supplementary data

Supplementary data related to this article can be found at http://dx.doi.org/10.1016/j.tet.2013.12.060.

References and notes

1. (a) Xing, P.; Li, S.; Xin, F.; Hou, Y.; Hao, A.; Sun, T.; Su, J. *Carbohydr. Res.* **2013**, *367*, 18–24; (b) Tsai, C. C.; Cheng, Y. T.; Shen, L. C.; Chang, K. C.; Ho, I. T.; Chu, J. H.; Chung, W. S. *Org. Lett.* **2013**, *15*, 5830–5833; (c) Liu, Z. X.; Feng, Y.; Yan, Z. C.; He, Y. M.; Liu, C. Y.; Fan, Q. H. *Chem. Mater.* **2012**, *24*, 3751–3757; (d) Svobodová, H.; Nonappa; Wimmer, Z.; Kolehmainen, E. *J. Colloid Interface Sci.* **2011**, *361*, 587–593; (e) Wang, X.; Zhou, L.; Wang, H.; Luo, Q.; Xu, J.; Liu, J. *J. Colloid Interface Sci.* **2011**, *353*, 412–419; (f) Díaz, D. D.; Kühbeck, D.; Koopmans, R. J. *Chem. Soc. Rev.* **2011**, *40*, 427–448.
2. (a) Li, Z.; Hao, A.; Hao, J. *Colloids Surf., A* **2014**, *441*, 8–15; (b) Liu, T.; Zhao, K.; Liu, K.; Ding, L.; Yin, S.; Fang, Y. *J. Hazard. Mater.* **2013**, *246–247*, 52–60; (c) van Herpt, J. T.; Stuart, M. C. A.; Browne, W. R.; Feringa, B. L. *Langmuir* **2013**, *29*, 8763–8767; (d) Zhang, C.; Wang, S.; Huo, H.; Li, Y.; Li, B.; Yang, Y. *Mater. Lett.* **2012**, *88*, 23–26; (e) Biradha, K.; Su, C. Y.; Vittal, J. *J. Cryst. Growth Des.* **2011**, *11*, 875–886.
3. (a) Bushby, R. J.; Lozman, O. R. *Curr. Opin. Solid State Mater. Sci.* **2002**, *6*, 569–578; (b) Hassheider, T.; Benning, S. A.; Kitzerow, H. S.; Achard, M. F.; Bock, H. *Angew. Chem., Int. Ed.* **2001**, *40*, 2060–2063; (c) Hird, M.; Goodby, J. W.; Hindmarsh, P.; Lewis, R. A.; Toyne, K. J. *Ferroelectrics* **2002**, *276*, 219–237; (d) Liu, C. Y.; Pan, H. Y.; Fox, M. A.; Bard, A. *J. Chem. Mater.* **1997**, *9*, 1422–1429.
4. (a) Kubo, W.; Kambe, S.; Nakade, S.; Kitamura, T.; Hanabusa, K.; Wada, Y.; Yanagida, S. *J. Phys. Chem. B* **2003**, *107*, 4374–4381; (b) Mitschke, U.; Bäuerle, P. *J. Mater. Chem.* **2000**, *10*, 1471–1507; (c) Pisula, W.; Menon, A.; Stepputat, M.; Lieberwirth, I.; kolb, U.; Tracz, A.; Sirringhaus, H.; Pakula, T.; Müllen, K. *Adv. Mater.* **2005**, *17*, 684–689; (d) van de Craats, A. M.; Stutzmann, N.; Bunk, O.; Nielsen, N. N.; Watson, M.; Müllen, K.; Chanzy, H. D.; Sirringhaus, H.; Friend, R. H. *Adv. Mater.* **2003**, *15*, 495–499; (e) Muccini, M. *Nat. Mater.* **2006**, *5*, 605–613.
5. (a) Luo, M.; Zhou, X.; Chi, Z.; Liu, S.; Zhang, Y.; Xu, J. *Dyes Pigm.* **2014**, *101*, 74–84; (b) Rajamalli, P.; Prasad, E. *Langmuir* **2013**, *29*, 1609–1617; (c) Bhalla, V.; Gupta, A.; Kumar, M.; Shankar Rao, D. S.; Krishna Prasad, S. *ACS Appl. Mater. Interfaces* **2013**, *5*, 672–679; (d) Kuang, G. C.; Jia, X. R.; Teng, M. J.; Chen, E. Q.; Li, W. S.; Ji, Y. *Chem. Mater.* **2012**, *24*, 71–80; (e) Perez, A.; Serrano, J. L.; Sierra, T.; Ballesteros, A.; de Saá, D.; Barluenga, J. *J. Am. Chem. Soc.* **2011**, *133*, 8110–8113; (f) Zhang, P.; Wang, H.; Liu, H.; Li, M. *Langmuir* **2010**, *26*, 10183–10190; (g) Kuang, G.; Ji, Y.; Jia, X.; Chen, E.; Gao, M.; Yeh, J.; Wei, Y. *Chem. Mater.* **2009**, *21*, 456–462.
6. (a) Dilovan, S. C.; Joan, R.; Jordi, R. A.; Helen, S. E. *Inorg. Chem.* **2004**, *43*, 1021–1030; (b) Yeşilel, O. Z.; Günay, G.; Mutlu, A.; Ölmez, H.; Büyükgüngör, O. *Inorg. Chem. Commun.* **2010**, *13*, 1173–1177; (c) Taşcıoğlu, S.; Aydın, A.; Yalcın, B.; Kakı, E.; Andac, Ö.; Büyükgüngör, O.; Koşar, B. *Polyhedron* **2011**, *30*, 2171–2180; (d) Garikoitz, B.; Oscar, C.; Antonio, L.; Urko, G. C.; Juan, P. G. T.; Pascual, R.; Luis, L. *Inorg. Chem. Commun.* **2003**, *6*, 1224–1227; (e) Wang, F. Q.; Zhuang, W. J.; Jin, L. P. *J. Mol. Struct.* **2007**, *832*, 48–54; (f) Lin, X. M.; Chen, L.; Fang, H. C.; Zhou, Z. Y.; Zhou, X. X.; Chen, J. Q.; Xu, A. W.; Cai, Y. P. *Inorg. Chim. Acta* **2009**, *362*, 2619–2626; (g) Güneş, G.; Okan, Z. Y.; Mustafa, S. S.; Seda, K.; Hakan, D. *Synth. Met.* **2011**, *161*, 2471–2480; (h) Meek, S. T.; Greathouse, J. A.; Allendorf, M. D. *Adv. Mater.* **2011**, *23*, 249–267; (i) Brunner, H.; Störikoa, R.; Rominger, F. *Eur. J. Inorg. Chem.* **1998**, 771–781.
7. Pieterse, K.; van Hal, P. A.; Kleppinger, R.; Vekemans, J. A. J. M.; Janssen, R. A. J.; Meijer, E. W. *Chem. Mater.* **2001**, *13*, 2675–2679.
8. Percec, V.; Aqad, E.; Peterca, M.; Rudick, J. G.; Lemon, L.; Ronda, J. C.; De, B. B.; Heiney, P. A.; Meijer, E. W. *J. Am. Chem. Soc.* **2006**, *128*, 16365–16372.
9. (a) Estroff, L. A.; Hamilton, A. D. *Chem. Rev.* **2004**, *104*, 1201–1217; (b) Sangeetha, N. M.; Maitra, U. *Chem. Soc. Rev.* **2005**, *34*, 821–836; (c) Suzuki, M.; Yumoto, M.; Kimura, M.; Shirai, H.; Hanabusa, K. *Chem.—Eur. J.* **2003**, *9*, 348–354.
10. Eldridge, J. E.; Ferry, J. D. *J. Phys. Chem.* **1954**, *58*, 992–995.
11. Liu, J. W.; Ma, J. T.; Chen, C. F. *Tetrahedron* **2011**, *67*, 85–91.
12. Cui, J.; Shen, Z.; Wan, X. *Langmuir* **2010**, *26*, 97–103.
13. Jung, J. H.; Shinkai, S.; Shimizu, T. *Chem.—Eur. J.* **2002**, *8*, 2684–2690.
14. Schmidt-Mende, L.; Fechtenkotter, A.; Mullen, K.; Moons, E.; Friend, R. H.; MacKenzie, J. D. *Science* **2001**, *293*, 1119–1122.
15. (a) Würthner, F.; Thalacker, C.; Diele, S.; Tschierske, C. *Chem.—Eur. J.* **2001**, *7*, 2245–2253; (b) Würthner, F.; Bauer, C.; Stepanenko, V.; Yagai, S. *Adv. Mater.* **2008**, *20*, 1695–1698; (c) Chung, J. W.; An, B. K.; Park, S. Y. *Chem. Mater.* **2008**, *20*, 6750–6755; (d) Shirakawa, M.; Kawano, S. I.; Fujita, N.; Sada, K.; Shinkai, S. *J. Org. Chem.* **2003**, *68*, 5037–5044.
16. (a) Kessler, H. *Angew. Chem., Int. Ed. Engl.* **1982**, *21*, 512–523; (b) Hamuro, Y.; Geib, S. J.; Hamilton, A. D. *J. Am. Chem. Soc.* **1996**, *118*, 7529–7541.
17. (a) Piepenbrock, M. O. M.; Lloyd, G. O.; Clarke, N.; Steed, J. W. *Chem. Commun.* **2008**, 2644–2646; (b) Zhang, Y. M.; Lin, Q.; Wei, T. B.; Qin, X. P.; Li, Y. *Chem. Commun.* **2009**, 6074–6076; (c) Teng, M.; Kuang, G.; Jia, X.; Gao, M.; Li, Y.; Wei, Y. *J. Mater. Chem.* **2009**, *19*, 5648–5654; (d) Lu, J.; Hu, J.; Song, Y.; Ju, Y. *Org. Lett.* **2011**, *13*, 3372–3375; (e) Huang, Y. D.; Dong, X. L.; Zhang, L. L.; Chai, W.; Chang, J. Y. *J. Mol. Struct.* **2013**, *1031*, 43–48.
18. (a) Frein, S.; Camerel, F.; Ziessel, R.; Barberá, J.; Deschenaux, R. *Chem. Mater.* **2009**, *21*, 3950–3959; (b) Li, C. Z.; Matsuo, Y.; Nakamura, E. *J. Am. Chem. Soc.* **2009**, *131*, 17058–17059; (c) Yin, J.; Qu, H.; Zhang, K.; Luo, J.; Zhang, X.; Chi, C.; Wu, J. *Org. Lett.* **2009**, *11*, 3028–3031; (d) Wang, X.; Zhou, Y.; Lei, T.; Hu, N.; Chen, E. Q.; Pei, J. *Chem. Mater.* **2010**, *22*, 3735–3745; (e) Cui, L.; Zhao, Y. *Chem. Mater.* **2004**, *16*, 2076–2082; (f) Ibtissam, T. D.; Nekelson, F.; Heinrich, B.; Donnio, B.; Guillon, D.; Kreher, D.; Mathevet, F.; Attias, A. J. *Chem. Mater.* **2011**, *23*, 4653–4656.
19. (a) Lin, K. T.; Kuom, H. M.; Sheu, H. S.; Lai, C. K. *Tetrahedron* **2013**, *69*, 9045–9055; (b) Gallardo, H.; Ferreira, M. *Tetrahedron* **2011**, *67*, 9491–9499.
20. Percec, V.; Bera, T. K.; Glodde, M.; Fu, Q.; Balagurusamy, V. S. K.; Heiney, P. A. *Chem.—Eur. J.* **2003**, *9*, 921–935.